WELDING RESEARCH

SUPPLEMENT TO THE WELDING JOURNAL, JANUARY 1974

Sponsored by the American Welding Society and the Welding Research Council

# Mössbauer - Effect Examination of Ferrite in Stainless Steel Welds and Castings

*Study shows feasibility of Mössbauer-effect scattering methods for obtaining baseline information on ferrite content of stainless steel welds and castings*

BY L. J. SCHWARTZENDRUBER, L. H. BENNETT, E. A. SCHOEFER, W. T. DELONG AND H. C. CAMPBELL

ABSTRACT. The differences between wholly austenitic, single phase stainless steels and those with two phase, partially ferritic structures have assumed commercial importance in recent years, but full utilization of the benefits to be derived from such two phase materials has been hampered by difficulties in establishing their exact ferrite contents.

The Mössbauer-effect scattering method measures the relative amounts of the austenite and ferrite phases on the basis of their magnetic properties in a way which is relatively independent of the shape, size and orientation of the ferrite particles. The method is nondestructive, requiring no special surface preparation, and thus can be directly compared with standard magnetic measurements. Utilizing backscattered 14 keV gamma rays, we have obtained for the first time Mössbauer spectra from a series of stainless steel welds and castings. The spectra have been carefully analyzed using correction factors developed for this purpose. This investigation establishes the procedures to provide base-line information for the calibration of instruments suitable for industrial use. Preliminary Mössbauer-effect results compare favorably with the assigned ferrite numbers for both the cast and weld materials for ferrite number less than about 20%, but give significantly lower values of ferrite content in the 30-50% ferrite range. The results also provide confirmation that ferrite in as-welded metal responds more strongly magnetically (as measured with the Magne-Gage) than an equal amount of ferrite in castings. Further development of the technique is necessary for firm quantitative conclusions.

Additional comments about cast austenitic alloys are presented in an appendix to this article.

*L. J. SCHWARTZENDRUBER and L. H. BENNETT are associated with the National Bureau of Standards, E. A. SCHOEFER is Consultant, Alloy Casting Institute Div., Steel Founders Society of America, W. T. DELONG is a Vice President, Teledyne Mc Kay and H. C. CAMPBELL, formerly with Arcos Corporation is now Manager of Education, American Welding Society.*
*Paper presented at the 54th AWS Annual Meeting held in Chicago during April 2-6, 1973.*

## Introduction

The presence of some ferrite in the microstructure of predominantly austenitic iron-chromium-nickel alloys has a significant influence on the physical and mechanical properties of the metal (Refs. 1-8). For example, partially ferritic stainless weld metals are more resistant to fissuring or cracking during or immediately after welding of heavy sections (Ref. 1). The physical properties of stainless steel castings also depend on the ferrite content. Improved welding characteristics, increased strength, and substantially greater resistance to stress-corrosion cracking are the chief attributes of the partially ferritic alloys in comparison to the wholly austenitic types. However, too much ferrite can decrease corrosion resistance (Ref. 3).

For these reasons, considerable effort has been expended on the development of consistent and reproducible measurement techniques of the absolute (or "true") ferrite con-

tent, none of which has, to date, proven to be entirely satisfactory. A standardized magnetic test procedure (Ref. 9) recently agreed upon by the Welding Research Council permits reliable intercomparison between measurements made at different laboratories. However, the relation of the assigned "ferrite numbers" to the true ferrite content is arbitrary to some extent and, although representing a good average based on existing commercial practice, it may be influenced by the shape, size, and orientation of the ferrite particles (Refs. 6-8).

Metallographic techniques for ferrite determination have been tried with various etchants and various counting techniques, x-ray diffraction has been attempted several times, magnetic saturation measurements have been made in Germany (Ref. 8) and France (Ref. 10), but none of these has been accepted by the Welding Research Council committee studying the problem of measuring ferrite, or the IIW Subcommission II-C, as being sufficiently accurate to justify accepting the resulting data as the true percent ferrite (Ref. 6,11). In addition, extensive round robins on weld metal specimens in the U.S. and Europe have shown that various magnetic instruments can differ appreciably in calibration. The range of values obtained is approximately from -40% to +60% of the average reading for the specimens tested (Ref. 11). However, the readings were self consistent from instrument to instrument, i.e., one instrument would read consistently higher or lower than another producing a smooth curve with rather low spread in readings if plotted versus another instrument.

Since many specifications for weld metal or castings require specific ferrite ranges, it was obvious that standardized instrument calibration was necessary. The Welding Research Council therefore recently agreed upon a procedure to standardize magnetic test methods (Ref. 9). This procedure utilizes NBS coating thickness standards as references for calibration and a Magne-Gage as the primary instrument. Other instruments may also be calibrated through the use of weld metal secondary standards. This procedure should satisfy the commercial need for reproducible results between laboratories directly for some types of instruments and through secondary standards for other types of instruments. However, a measure of the true or absolute ferrite content of weld and cast metals is still desirable.

Precision in ferrite content measurement in determining the influence of each constituent in the alloy on the amount of ferrite obtained is needed, for example, since the foundryman must juggle his composition correctly if he is to meet a ferrite range specification. As the ferrite content of cast alloys of the 19Cr, 9Ni type is increased from zero to about 35%, the average yield strength is increased by 50% or more (Ref. 4). As a further example, the stress required to initiate cracking in a stress-corrosion cracking medium such as sodium chloride is increased from around five thousand psi for wholly austenitic alloys to over thirty thousand psi for alloys containing ferrite in the 30 to 40% range (Ref. 4). All of the ferrite-containing cast alloys show less susceptibility to cracking upon welding than the ferrite-free alloys, and weld deposits containing ferrite show a similar reduction in fissuring tendency. However, too much ferrite leads to the brittleness associated with sigma phase formation (Ref. 2) and for both welds and cast steels can have deleterious effects on corrosion resistance (Refs. 3-5).

We report here an investigation concerning the applicability of the Mössbauer-effect scattering method to the problem of ferrite in austenite determination in bulk materials. In principle, this method offers a highly accurate and self-characterizing means for determining the relative amounts of ferrite and austenite. As with the more conventional magnetic test methods, the Mössbauer method measures the relative amounts of austenite and ferrite phases on the basis of their magnetic properties, but in a way which is relatively independent of the shape, size and orientation of the ferrite particles. The scattering method is nondestructive and requires no special surface preparation and can thus be directly compared with the conventional magnetic measurements. This investigation is concerned with the techniques and procedures required to develop Mössbauer instruments suitable for industrial and laboratory use. Some preliminary measurements are reported on cast and weld samples. These results indicate that, with further refinement, Mössbauer scattering with its unique advantages should be useful in providing base-line information for the calibration of standards and instruments for field use in terms of true ferrite content. There is presently no single method, whether x-ray diffraction, quantitative metallography, magnetic saturation, or Mössbauer scattering, which has proven capability for sufficiently reliable measurements, and therefore it would be preferable to use a combination of methods in order to determine and verify the true ferrite content.

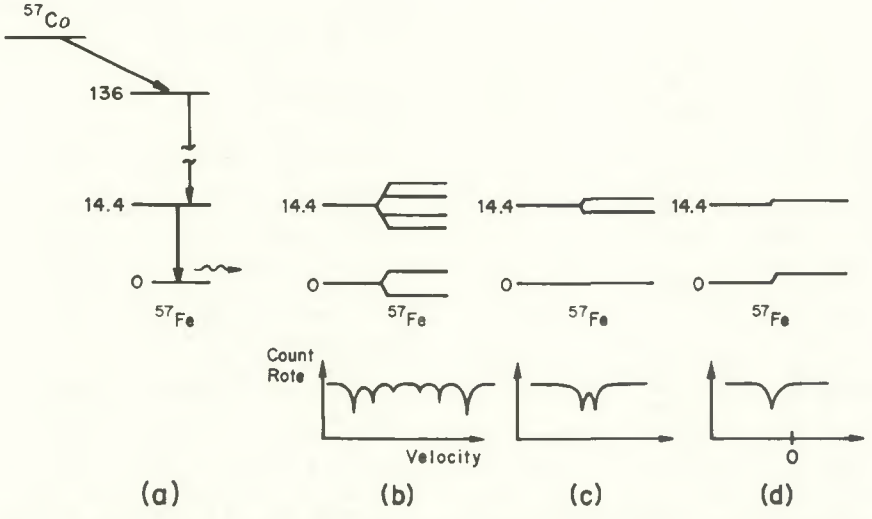


*Fig. 1 — (a) Decay scheme of radioactive Co-57 which is used as the source of 14.4 keV γ rays. The Co-57 is incorporated in a matrix such as Pd which gives a narrow unsplit source line.*

*(b) Magnetic splitting of the ground and first excited state of an Fe-57 nucleus, as for example in ferrite. Of the eight possible transitions, two are forbidden, giving a six-line spectrum, as shown.*

*(c) Splitting of the first two levels of an Fe-57 nucleus in an electric field gradient, giving a two-line spectrum.*

*(d) Shift of the levels due to the charge of electrons at the nuclear site. A spectrum displaced from the zero of velocity results. This displacement is termed the "isomer shift". For (b) or (c) the displacement of the entire pattern is a measure of the isomer shift*

## Mössbauer Technique

The Mössbauer effect is a technique for observing resonant nuclear gamma ray fluorescence in solids. Efficient observation of the effect depends on details of nuclear structure and is thereby limited in application to a relatively few isotopes. Prom-

inent among these is Fe-57, for which the radiation decay scheme is illustrated in Fig. 1(a). Also illustrated are the effects of a magnetic field, Fig. 1(b), an electric field gradient, Fig. 1(c), and the electron charge density, Fig. 1(d), on the observed Mössbauer spectrum. The Mössbauer effect is able to distinguish different phases in a material on the basis of variations of these three effects (Refs. 12-14), and a number of studies in stainless steels and other Fe alloys have been reported (Refs. 15-25).

An experimental arrangement for observation of the Mössbauer effect is shown in Fig. 2. A lead shield with a brass tube lined hole serves to collimate the gamma ray beam and to shield the scattering detector from the primary beam. A radioactive source containing Co-57 (which decays to Fe-57 with a 270 day half life) is imparted a linear motion by a velocity transducer. Radiation, either transmitted through or scattered by the sample under study, is detected by appropriately placed counters. The purpose of the brass tube is to prevent fluorescent x-rays originating in the lead shield from interfering with efficient detection of 14.4 keV gamma rays. The x-ray fluorescence is due mainly to the presence of a 122 keV gamma ray which precedes every 14.4 keV gamma ray. Aluminum filters are used to reduce the number of lower energy x-rays incident on the counter. Proportional counters containing Xe-$CO_2$ or Kr-$CO_2$ are efficient for detecting the 14.4 keV gamma rays. The motion imparted to the source by the velocity transducer alters the energy of the gamma rays by the Doppler effect. This change in energy is very small and is detectable only by observing the resonance fluorescence. When the resonance condition is satisfied, there is a decrease in the transmitted radiation and an increase in the scattered radiation, as illustrated in Fig. 2(b).

Transmission is the most efficient method for obtaining Fe-57 Mössbauer spectra. However, for materials containing predominantly Fe, Cr, and Ni, the transmission method is useful only for samples thinner than about 125 $\mu$m (0.005 in.). For thicker samples the scattering method must be used. Transmission spectra are obtained by detecting the 14.4 keV gamma rays. Scattering spectra can be obtained by detecting either (1) the 14.4 keV gamma rays, (2) 6.3 keV x-rays, or (3) internal conversion electrons. The latter two are possible since a large fraction of the decays from the Fe-57 excited nuclear level are via internal conversion processes, whereby the decay energy of the excited nuclear state is used to expel a K-shell electron from the Fe atom. For detecting 6.3 keV x-rays, the filtering arrangement shown in Fig. 2 should be modified, e.g., by placing the aluminum filter in front of the sample. An Ar-$CO_2$ proportional counter is advantageous because it is inefficient at 14.4 keV and higher energies. For detecting the conversion electrons, a special counter utilizing He-$CH_4$ gas directly in contact with the sample (Ref. 26) can be used. Spectra obtained with either the 14.4 keV gamma rays or the 6.3 keV x-rays represent a sampling of a region about 100 $\mu$m (about 0.004 in.) thick at the surface of the sample, whereas spectra from conversion electrons sample to a depth of only about 1 $\mu$m. Conversion electron spectra are therefore useful for detecting metallurgical differences between surface layers and the bulk metal (Ref. 27). In this paper we have restricted ourselves to spectra obtained utilizing the 14.4 keV gamma rays (although some simultaneous detection of the 6.3 keV x-rays was probably present). Further development of the technique will undoubtedly involve the other two detection methods as well.

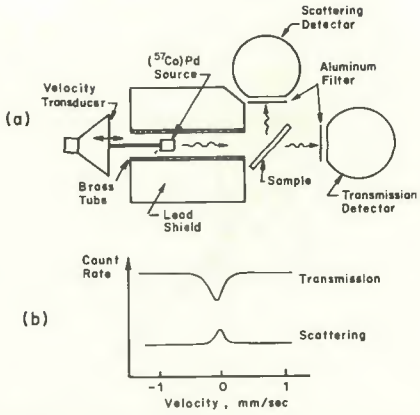


*Fig. 2 — (a) Experimental arrangement for observing the Mössbauer effect by scattering or transmission, for a thin sample. The scattering experiment can also be performed on a thick sample. For efficient scattering experiments, source strengths greater than about 50 mCi are desirable. For transmission, sources with about 10 mCi or less are suitable*

*(b) Schematic comparison of spectra obtained by transmission and by scattering.*

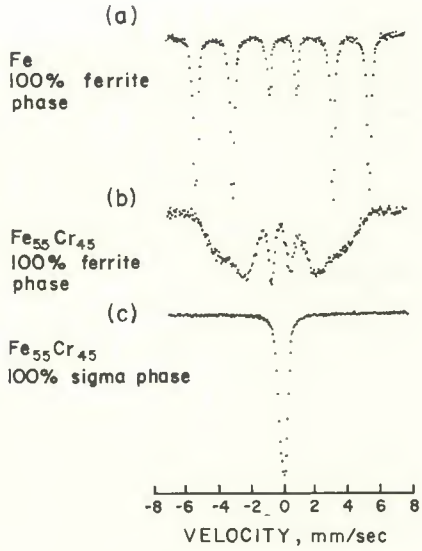


*Fig. 3 — Experimental Mössbauer transmission spectra for (a) a pure iron foil, (b) an alloy containing 55 at. % Fe and 45 at. % Co after annealing at 1000 C for one hour and quenching to room temperature to form single-phase ferrite and (c) the same alloy after annealing at 775 C for 10 days to produce sigma phase. No trace of ferrite is seen in spectrum (c)*

## Quantitative Measurement of the Ferrite Content Using the Mössbauer Effect

When different phases in a metal give well-resolved Mössbauer spectra, the relative areas of the spectral patterns provide an indication of the amount of each phase present. An example of the Mössbauer spectra for two distinct phases in an iron-chromium (45 at .% Cr) alloy is shown in Fig. 3(b,c) and compared with the spectrum of pure iron in Fig. 3(a). The disordered (magnetic) and sigma (nonmagnetic) phases in the Fe-Cr alloy clearly give two distinct spectral patterns and the composite spectrum from an alloy consisting of a mixture of these two phases could be resolved. Figure 4 compares the spectrum from the same sigma phase with that from an austenitic stainless steel. Due to the expanded velocity scale, the structure of the sigma phase spectrum is more readily apparent in Fig. 4(a) than in Fig. 3(c). Although these spectra are not as distinct as in the previous case, under favorable circumstances the fraction of sigma phase in a stainless steel might be measurable.

At present, no detailed studies have appeared concerning the accuracy and precision obtainable in quantitative metallographic studies of steels using the Mössbauer method. The first consideration is the accuracy with which the relative area fractions can be obtained from the Mössbauer spectrum. This requires both a good signal-to-noise ratio and the ability to separate geometric effects from resonance effects. The conversion of spectral area fractions to phase fractions requires corrections for finite thickness effects, phase composition, and differing recoil-free fractions.

Finite thickness corrections have been considered by a number of authors for the case of transmission spectra (Refs. 28-32). For scattering spectra, Chow and Bogner (Ref. 25),

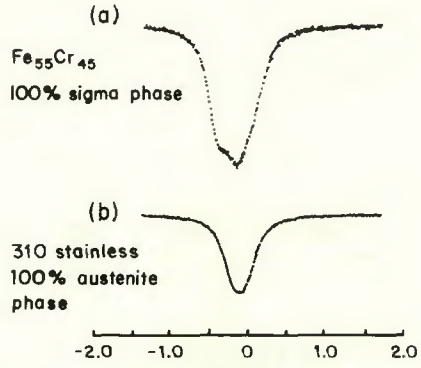


*Fig. 4 — Comparison of Mössbauer transmission spectra from an Fe-Cr σ phase sample and an austenitic stainless steel. The spectrum in (a) is obtained on the same sample whose spectrum is shown in Fig. 3c, but with an expanded velocity scale*

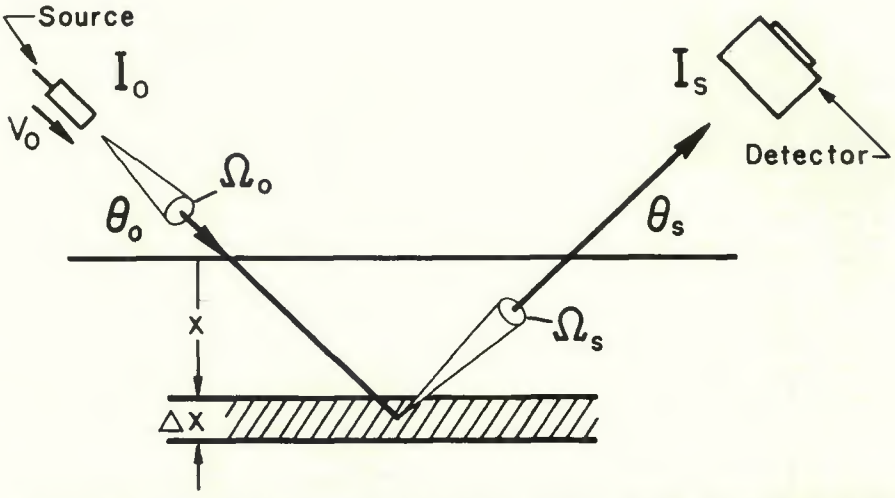


*Fig. 5 — Geometry for a Mössbauer scattering experiment. A source of gamma rays is given a velocity $v_o$. The incident gamma rays subtend a solid angle $\Omega_o$. The radiation scattered into solid angle $\Omega_s$ is counted by the detector*

have discussed the quantitative measurement of small amounts of retained austenite in ferrite. They utilized an empirical formula with parameters adjusted to give agreement with x-ray results. This formula cannot be extended for use with large amounts of austenite and we have proceeded to investigate the necessary correction factors. This was done specifically for a single line source and a sample with well resolved absorption lines.

Consider the scattering geometry shown in Fig. 5. A source emitting $I_o$ recoil-free gamma rays per second is imparted a velocity $V_o$ in the direction of gamma ray propagation. This incident beam is collimated to subtend a solid angle $\Omega_o$. The intensity $i_o(E,V_o)$ of recoil-free gamma rays of energy E incident on a layer of material at a distance x below the surface will be:

$$i_o(E,V_o) = I_o \frac{\Omega_o}{4\pi} u(E,V_o)$$

$$\exp\left\{-[\alpha_{at}+g(E)]x/\cos\theta_o\right\}, \qquad (1)$$

where $u(E,V_o)$ is the energy distribution of recoilless radiation from the source, $\alpha_{at}$ is the inverse atomic absorption length for 14 keV gamma rays, g(E) is the inverse resonant absorption length for gamma rays of energy E, and the other symbols are as defined in Fig. 5. The quantities u and g can be represented by the Lorentzian functions:

$$u(E,V_o) = \frac{2}{\pi\Gamma_s}\frac{1}{(2/\Gamma_s)^2(V_E-V_o-V_{IS})^2+1}, \qquad (2)$$

and

$$g(E) = \frac{n f_a \sigma_o (\Gamma_o/\Gamma_a)}{(2/\Gamma_a)^2(V_E-V_{IA})^2+1} \qquad (3)$$

where $\Gamma_s$ is the full width at half maximum (FWHM) of the source, $\Gamma_a$ the FWHM of the sample absorption line under consideration, $\Gamma_o$ is the natural FWHM (0.19 mm/sec), n is the number of Fe-57 atoms per $cm^3$ which contribute to the resonance, $\sigma_o$ is the effective cross section for resonant absorption, $f_s$ is the recoilless fraction for the sample, $V_E$ is the velocity corresponding to a gamma ray of energy E, and $V_{IS}$ and $V_{IA}$ are the shifts of the gamma ray line due to hyperfine fields. In Eq. 3 it has been assumed that, whatever mechanism is present to broaden the absorption line, a nearly Lorentzian shape is preserved. This is a good approximation even in the presence of considerable broadening.

The detector system can, in principle, be tuned to detect either 14 keV gamma rays, 6.3 keV x-rays arising from the internal conversion process, or the conversion electrons. Consider first the case of detecting 14 keV gamma rays. Resonant reabsorption of the gamma rays scattered towards the detector must be considered. The intensity of radiation of energy E' arriving at the detector from a depth x in the sample due to incident radiation of energy E will be given by

$$i_{a_o}(E',E,V_o) = \frac{\Omega_s}{2\pi^2\Gamma_a(1+\alpha)} i_o(E,V_o)$$

$$g(E)\frac{g(E')}{n f_a \sigma_o \Gamma_o/\Gamma_a}$$

$$\exp\left\{-(\alpha_{at}+f_a g(E'))x/\cos\theta_s\right\}, \qquad (4)$$

where $\alpha$ is the internal conversion coefficient. In the case of a phase such as ferrite, with a six line absorption pattern, g(E') will consist of six Lorentzians with the form of Eq. (6), each with an appropriate weighting factor. For randomly oriented ferrite, the six lines have an intensity ratio of 3:2:1:1:2:3. The presence of any preferred orientation will change this ratio (and thus have an influence on the calculated correction factors). After integrating Eq. (4) over E', one obtains, for a single line spectrum

$$i_{ao}(E,V_o) = \frac{\Omega_s}{4\pi}\frac{1}{(1+\alpha)} i_o(E,V_o) g(E)$$

$$\exp\left\{-(\alpha_{at}+\tfrac{1}{2}f_a\alpha_r)x/\cos\theta_s\right\}$$

$$I_o(\tfrac{1}{2}f_a\alpha_r x/\cos\theta_s) \qquad (5)$$

where $I_o$ is a modified Bessel function of zero order and $\alpha_r = n f_a \sigma_o \Gamma_o/\Gamma_a$.

Further analytical integration is complicated by the presence of the Bessel function. However, if it is assumed that the most important contribution to the spectrum arises from the first few absorption lengths, then $\exp(-\tfrac{1}{2}f_a\alpha_r x/\cos\theta_s)\, I_o(\tfrac{1}{2}f_a\alpha_r x/\cos\theta_s)$ can be approximated as $\exp(-\tfrac{1}{2}f_a\langle\alpha_r\rangle x/\cos\theta_s)$, where

$$\langle\alpha_r\rangle \approx 0.8\langle n\rangle f_a\sigma_o\Gamma_o/\Gamma_a. \qquad (6)$$

Here in order to include the case of a multi-line absorption spectrum, $\langle n\rangle$ is introduced as the effective number of Fe-57 nuclei per $cm^3$ for the phase in question. For a single line spectrum $\langle n\rangle = n$. For the case of a multiline spectrum $\langle n\rangle$ is reduced by the average of the squared probabilities for re-emission in any of the lines (e.g., for a 3:2:1:1:2:3 ferrite pattern, $\langle n\rangle \approx 0.032$). With this approximation, and for $\theta_s = \theta_o$, one obtains from Eq. (5) by integration over x the total resonant count rate at the detector, for the source with velocity $V_o$, as

$$I_s(V_o) = I_o \frac{\Omega_o\Omega_s C}{16\pi^2(1+\alpha)} \frac{1}{(2/\Gamma)^2[V_o-(V_{IS}-V_{IA})]^2+1} \qquad (7)$$

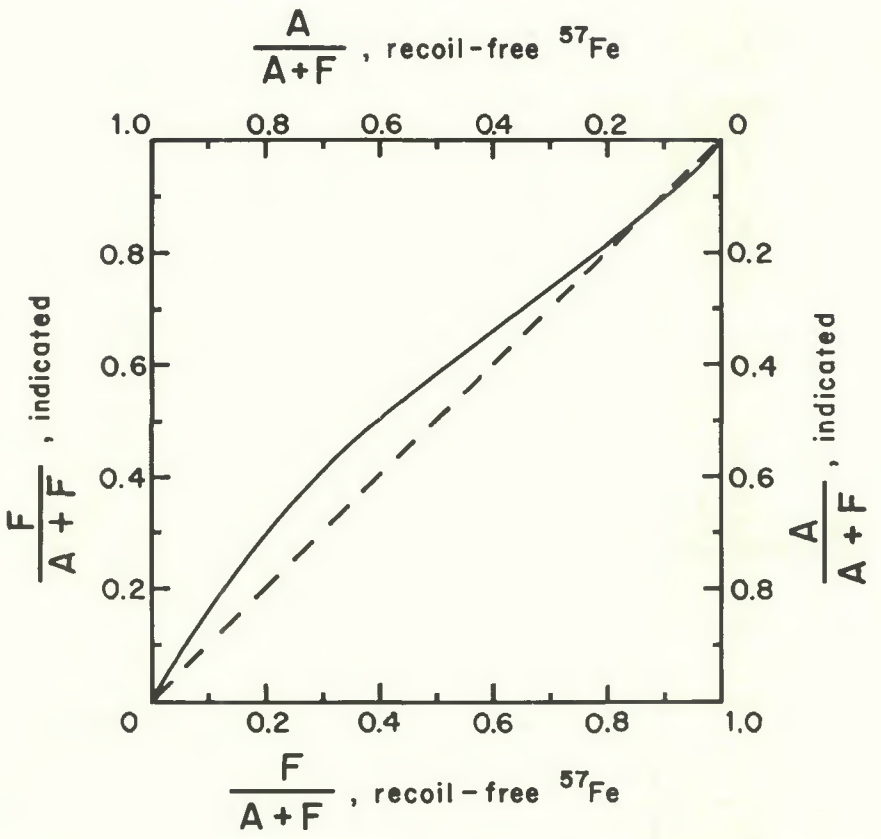


*Fig. 6 — The fraction of Fe-57 in the ferrite phase, F/(A+F), as indicated from the relative areas of ferrite, F, and austenite, A, in the Mössbauer spectrum versus the fraction of recoil-free Fe 57 actually present in the ferrite phase. The dashed line (slope = 1) would apply in the absence of thickness effects. The curve applies when scattered 14.4 keV γ rays are being detected. Derivation involves a number of assumptions, as described in the text. To obtain the weight fraction of ferrite, further correction for recoil-free fraction and phase composition is necessary, and to obtain the volume fraction, a density correction is also required.*

with

$$C = \frac{\alpha_r \Gamma_a}{2\alpha_{at} F_1 F_2 \Gamma} \quad (8)$$

$$\Gamma = \Gamma_s + F_1 \Gamma_a \quad (9)$$

$$F_1 = \left[1 + \frac{\alpha_r}{2\alpha_{at} + \frac{1}{2}\langle\alpha_r\rangle}\right]^{\frac{1}{2}} \quad (10)$$

$$F_2 = 1 + \frac{\langle\alpha_r\rangle}{4\alpha_{at}} \quad (11)$$

This is a Mössbauer spectrum with the Lorentzian shape preserved, but with a broadened FWHM. From Eq. (7), the total area $A_a$ under this resonance line in the spectrum will be, when 14.4 keV gamma rays are detected,

$$A_a^{14.4} = I_o \frac{\Omega_o \Omega_s}{32\pi(1+\alpha)} \frac{nf_a \sigma_o \Gamma_o}{2\alpha_{at} F_1 F_2} \quad (12)$$

If 6.3 keV x-rays are counted by the detector then Eq. (12) becomes

$$A_a^{6.3} = I_o \frac{\Omega_o \Omega_s \alpha}{32\pi(1+\alpha)} \frac{nf_a \sigma_o \Gamma_o}{(\alpha_{at}^{14.4} + \alpha_{at}^{6.3}) F_1^{6.3}} \quad (13)$$

with

$$F_1^{6.3} = \left[1 + \frac{\alpha_r}{\alpha_{at}^{14.4} + \alpha_{at}^{6.3}}\right]^{\frac{1}{2}} \quad (14)$$

where $\alpha_{at}^{14.4}$ and $\alpha_{at}^{6.3}$ are the inverse atomic absorption lengths for 14.4 and 6.3 keV radiation, respectively. If conversion electrons are counted by the detector, then Eqs. (13) and (14) apply with $\alpha_{at}^{6.3}$ replaced by the inverse absorption length appropriate for conversion electrons, $\alpha_{at}^{el}$.

Consider the case for the presence of two phases, a ferrite phase F and an austenite phase A. The experimental quantity obtained from the Mössbauer spectrum is the ratio of the areas for the two spectra corresponding to austenite and ferrite. The austenite spectrum can be considered as a single line, whereas the ferrite yields a six-line pattern. For later use, we have used Eq. (12) to generate a correction factor curve assuming: (1) only 14.4 keV gamma rays are being detected, (2) $\Gamma \approx 0.25$ mm/sec for the austenite and $\Gamma_a \approx 2.0$ mm/sec for the ferrite, (3) the ferrite lines are in the ratio 3:2:1:1:2:3, and (4) $f_a = 0.8$ for both the ferrite and the austenite. Also used were the parameters $\alpha_a = 0.52 \times 10^3 cm^{-1}$, $\sigma_o = 2.56 \times 10^{18} cm^2$, $\Gamma_o = 0.20$ mm/sec, and 2.19% for the isotopic abundance of Fe-57. Using these values, the correction factor curve plotted in Fig. 6 is obtained. With this curve, the ratio of area fractions F/(A+F) obtained from the Mossbauer spectrum can be corrected for finite thickness effects. The relative atomic fraction of recoil-free Fe in each phase is thereby obtained.

To obtain the relative phase fractions, corrections for recoil-free fraction and phase composition are also required. The recoil-free fractions in the various alloy compositions encountered in ferritic stainless steels have not been precisely determined. However, recent measurements by Qaim (Ref. 33) for the recoil-free fraction yielded f=0.81, 0.76, and 0.76 for Fe-57 in Ni, Cr, and Fe, respectively. On this basis, the correction for recoil-free fraction is expected to be small, on the order of a few percent, and can be neglected for practical purposes. Correction for phase composition is important (though less a problem than in the magnetic saturation method) for the higher ferrite concentration alloys and is discussed in the next section.

## Experimental Measurements

A series of measurements using the Mössbauer technique was performed on five stainless steel castings and four stainless steel welds (Ref. 34). The compositions of these samples are detailed in Table 1, which also shows the Cr and Ni equivalents used to obtain an indicated v/o ferrite from constitution diagrams. The shapes and dimensions of these samples are illustrated in Fig. 7.

An existing Mössbauer spectrometer was modified for use in the scattering mode with an arrangement similar to that shown in Fig. 2. The detector was a Xe-$CO_2$ proportional counter. The single-line source was approximately 50 mCi of Co-57 in Pd. The window of a single channel analyzer was adjusted to detect primarily the 14.4 keV scattered radiation. This adjustment is rather critical since the resolution of the counting system gives some overlap between the two energies and there are about eight times as many 6.3 keV x-rays as 14.4 keV gamma rays. Thus detecting only about 10% of the x-rays would give a correction factor intermediate between those of Eq. (12) and Eq. (13). The Al filter placed as shown in Fig. 2, is an aid in reducing the number of x-rays counted. Although subsequent experience may require modification, we have proceeded on the basis that only a negligible fraction of the x-rays were being counted, and the correction factor

**Table 1 — Composition of Samples (in weight percent)**

| Sample code | Alloy type | C | Si | Mn | Cr | Ni | Mo | N | Schoefer cast steel diagram[a] Cr Equiv. | Ni Equiv. | Weld metal diagrams Schaeffler[b] Cr Equiv. | Schaeffler[b] Ni Equiv. | Delong[c] Cr Equiv. | Delong[c] Ni Equiv. |
|---|---|---|---|---|---|---|---|---|---|---|---|---|---|---|
| Cast samples | | | | | | | | | | | | | | |
| A 2 | CF-8M | 0.08 | 1.12 | 0.85 | 16.72 | 15.02 | 2.51 | 0.042 | 15.92 | 21.19 | | | | |
| C 2 | CF-8 | 0.07 | 1.25 | 0.80 | 19.99 | 9.38 | — | 0.062 | 16.83 | 15.75 | | | | |
| D 2 | CF-8M | 0.07 | 1.39 | 0.79 | 20.17 | 9.55 | 2.40 | 0.064 | 19.67 | 15.96 | | | | |
| F 2 | CF-3M | 0.026 | 1.43 | 0.91 | 20.31 | 10.86 | 2.59 | 0.04(est.) | 20.06 | 15.39 | | | | |
| K 2 | CE-30A | 0.30 | 0.91 | 0.82 | 28.93 | 8.34 | — | 0.120 | 25.31 | 23.12 | | | | |
| Weld samples[d] | | | | | | | | | | | | | | |
| 52 D | 308 | 0.053 | .73 | 1.00 | 20.10 | 10.11 | .16 | .058 | | | 21.35 | 12.20 | 21.35 | 13.94 |
| 6 B | 308 | 0.047 | .31 | 1.69 | 20.60 | 9.97 | .17 | .046 | | | 21.23 | 12.23 | 21.23 | 13.61 |
| 8 B | 308 | 0.047 | .31 | .90 | 21.70 | 9.85 | .17 | .046 | | | 22.33 | 11.71 | 22.33 | 13.09 |
| 12 H | None | 0.05 | .38 | .90 | 22.65 | 9.80 | 2.47 | .046 | | | 25.69 | 11.75 | 25.69 | 13.13 |

(a) See Appendix and also Beck et al., Ref. 4.
(b) Schaeffler, A. L., "Constitution Diagrams for Stainless Steel Weld Metal," Metal Progress *56*, p. 680 (1949).
(c) DeLong, W. T., Ostrom, G. A., and Szumachowski, E. R., "Measurement and Calculation of Ferrite in Stainless-Steel Weld Metal," Welding Journal, p. 521-s, 1956.
(d) Compositions for the four weld samples are estimated, not actuals.

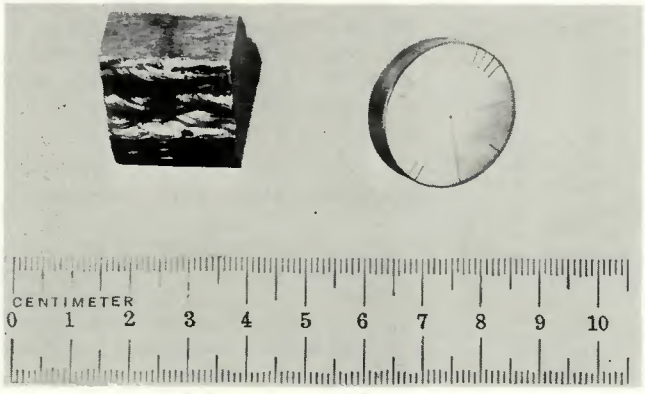


*Fig. 7 — Weld and cast materials used in this study. The weld sample (on the left) was one of a set of standards provided by Teledyne McKay, and the cast sample (on the right) one of a set provided by Prof. F. H. Beck of Ohio State University*

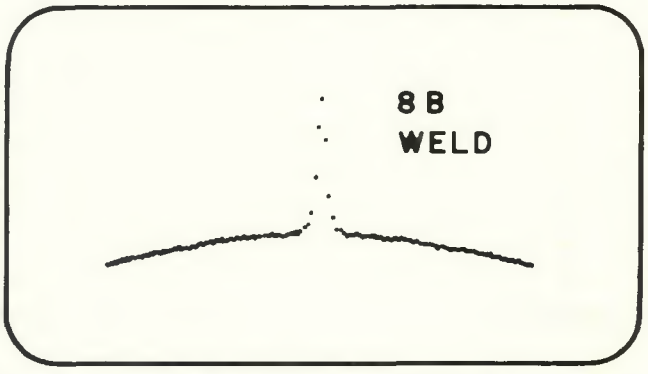


*Fig. 8 — Spectrometer oscilloscope readout for scattering from weld sample No. 8B without any data reduction. The curved background is partially due to changes in the solid angle, $\Omega_o$, Fig. 5, (resulting from source motion) and partially to an unresolved ferrite spectrum. Note that in scattering, as shown here, increases in count rate are observed in contrast to transmission, e.g., Figs. 3 and 4, where decreases are observed*

curve shown in Fig. 6 will be used.

The spectrum from weld sample 8B as it appeared on the oscilloscope of the spectrometer is shown in Fig. 8. The predominant peak in the center is from the austenite phase. The curved background is primarily a geometric effect due to the source motion. (During one cycle of operation the source is swept through the entire range of velocities. The repetition rate is about 2 cycles per second. For velocities near zero the source is nearer the detector, where it produces a higher count rate.) The ferrite spectrum, only barely visible due to the presence of the curved background, is a broadened six-line spectrum similar to that shown in Fig. 3(b) for a ferritic Fe-Cr alloy.

Before making further analysis, the data were reduced by subtracting out the background curvature. This was accomplished by fitting to a parabola that portion of the spectrum with absolute velocities greater than about 7.5 mm/sec using a least-squares technique. Contributions due to resonance effects are small in this region of the spectrum. This parabola was then subtracted from the entire spectrum, yielding a flat background as shown in Fig. 9. In these spectra, especially that for sample K2, the ferrite contribution is evident. (Each of these spectra represent approximately 48 h counting time on the spectrometer.) The error introduced by the background reduction procedure is believed to be small but is difficult to assess. More satisfactory would be a reduction by experimental means. This could be accomplished, for example, by using a spectrometer with a higher frequency capability (i.e. a higher repetition rate), by using an increased source-to-sample distance (requiring a stronger radiation source), or by using a spectrometer with a specialized constant velocity capability.

After removal of the geometric background, the residual data were least-squares fitted to the sum of a single line spectrum corresponding to the austenite, and a broadened six line spectrum corresponding to the ferrite.

A computerized least-squares fitting routine, similar to that described by Chrisman and Tumolillo (Ref. 35) which seeks a least-squares minimum by successive iteration, was utilized. The single line austenite spectrum was assumed to be of Lorentzian shape. The ferrite spectrum was assumed to arise from a

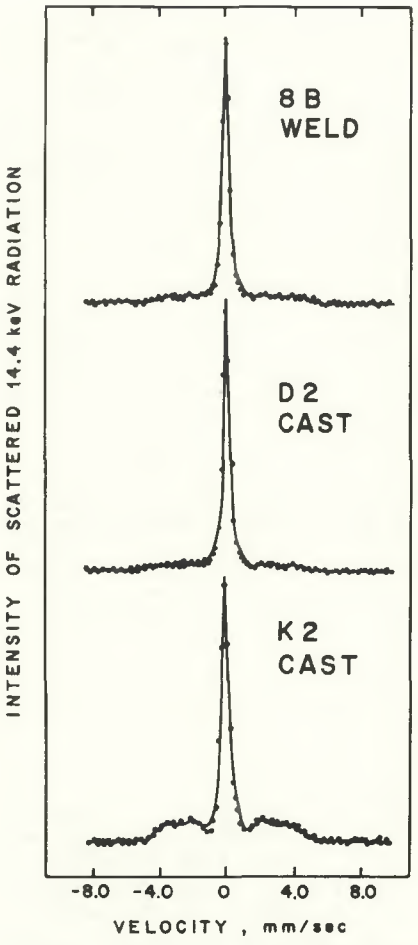


*Fig. 9 — Mössbauer scattering spectra from three samples after computer analysis. The dots are experimental data from which the curved portion of the background due to source motion has been subtracted. The solid lines are a least-squares fit to a broad spectrum due to ferrite, and to a narrow spectral line in the center due to austenite*

**Table 2 — Parameters Obtained in a Least-Squares Fit to Mössbauer Scattering Spectra from a Series of Weld and Cast Stainless Steel Samples [a]**

| Sample code | $H_o$ kG | $\sigma_H$ kG | Austenite Line FWHM,[c] mm/sec | F/A |
|---|---|---|---|---|
| Cast samples | | | | |
| A 2 | 235[b] | 50[b] | 0.47(2) | 0.04(3) |
| C 2 | 230(8) | 50(6) | 0.45(2) | 0.13(2) |
| D 2 | 232(8) | 47(6) | 0.47(2) | 0.24(2) |
| F 2 | 222(10) | 51(4) | 0.46(2) | 0.42(3) |
| K 2 (run no. 1) | 219(8) | 44(6) | 0.46(2) | 0.80(4) |
| (run no. 2) | 225(10) | 40(4) | 0.49(2) | 0.89(4) |
| Weld samples | | | | |
| 52D | 226(19) | 32(18) | 0.45(2) | 0.15(3) |
| 6B | 229(16) | 26(15) | 0.45(2) | 0.16(3) |
| 8B | 226(8) | 51(8) | 0.49(2) | 0.25(4) |
| 12H | 232(10) | 51(10 | 0.43(2) | 0.30(4) |

(a) F/A is the ratio of the spectral area due to the ferrite to that due to the austenite. Numbers in parentheses represent estimated statistical errors for the least-squares fit at the one sigma level.
(b) Assumed values held constant during the fitting procedure.
(c) FWHM = Full width of half maximum

Gaussian distribution of magnetic hyperfine fields, each with a six-line pattern with a 3:2:1:1:2:3 intensity ratio and line widths of 0.30 mm/sec. The relative probability, p(H), for a given magnetic hyperfine field H, is then

$$p(H) = A \exp[-(H-H_0)^2/2\sigma_H^2] \qquad (15)$$

Initial values must be assumed for each parameter of the fit. If the initial values deviate too much from the true values, the iterative least squares procedure will diverge, or converge to nonsensical values. Further, it was found necessary to independently vary the parameters for the austenite and ferrite portions of the spectra. After fitting the ferrite and austenite spectra, their small contribution to the background could be calculated and a more precise fit of the background curvature could be accomplished. This was done in each case, followed by another sequence of data reduction and of ferrite and austenite spectral area calculation. As can be seen in Fig. 9, the fits are not quite satisfactory near the base of the large austenite line, probably because of the overlap of the austenite and ferrite spectra. The area of the misfit amounts to only a few percent of either the austenite or the ferrite area, and should not introduce errors greater than this amount. The results of least-squares fitting of the experimental data are given in Table 2.

Tabulated in Table 3 are the Mössbauer results and the ferrite numbers determined on the same set of samples using the Welding Research Council procedure (Ref. 9). Also tabulated are the ferrite contents indicated on constitution diagrams and, for the cast samples, metallographic determinations. The corrected Mössbauer results give the atomic percent of the total recoil-free iron appearing in the ferrite phase. As mentioned previously, the recoil-free fractions are expected to be equal within a few percent. If the recoil-free fraction, the a/o iron, and the atomic density were the same in the ferrite and austenite phases, the corrected Mössbauer results of Table 3 would be directly comparable to the v/o ferrite and hence, presumably, to the ferrite number. All three of these corrections are, in fact, small.

Bungart et al (Ref. 8) found that, on the average the ferrite phase is enriched in chromium by about 25% and impoverished in nickel by about 30% with respect to the composition of the matrix. Using these figures, consider sample F2 which contains 20.3% Cr and 10.8% Ni and is about 30% ferrite. The ferrite phase would contain about 68% iron and the austenite phase about 70% iron, requiring only a 2% correction in the Mössbauer results. The magnitude of the magnetic hyperfine field could be used to give a measure of the ferrite phase composition if the effect of alloying on the hyperfine field values were well established. The hyperfine field as a function of composition has been measured for binary Fe-Cr alloys by Yamamoto (Ref. 36) and for binary Fe-Ni alloys by Johnson et al (Ref. 37). Similar data are not yet available for Fe-Cr-Ni ternary alloys.

However, Bungart et al (Ref. 8) found that, for ternary alloys with greater than about 20% Cr, the saturation magnetization depends on the sum of the alloying elements Cr + Ni. Since the Fe-57 magnetic hyperfine field in iron alloys is often roughly proportional to the magnetization, we assume as a rough approximation that the magnetic properties of the ferrite phase depend on the total Cr + Ni content. Then, using the results of Yamamoto (Ref. 36) the graph in Fig. 10b can be constructed. Comparison with the measured hyperfine fields (Fig. 10a) shows that, on the average, the ferrite phase contains about 38 atomic percent Cr + Ni. This is in the same direction as that found by Bungart et al (Ref. 8), i.e. there is an increase in Cr + Ni content in the ferrite phase over that in the austenite phase. However, the absence of knowledge of the hyperfine field in ternary alloys, precludes their direct use.

From the values given by Pearson (Ref. 38) for the lattice spacings of the austenite and ferrite phases, the atomic density (i.e., no. of atoms per $cm^3$) is about 2% smaller for the ferrite phase than for the austenite phase. Again this is a small correction to the Mössbauer results.

The ferrite content measured by the Mössbauer effect, corrected for finite thickness effects as shown in Table 3, is compared graphically with the ferrite number in Fig. 11. Addi-

Table 3 — Ferrite Content from Mossbauer Measurements Compared with Ferrite Number and Indicated Ferrite from Alloy Chemistry

| Sample code | Indicated V/O ferrite from constitution diagrams: Schoefer cast steel | Schaeffler weld metal | Metallographic V/O ferrite[b] | Ferrite number, DeLong weld metal diagram[a] | Magne-Gage ferrite number[c] | Mössbauer results: Mössbauer ferrite area ratio 100×F/(A+F) | Mössbauer results: Corrected for finite thickness[e] |
|---|---|---|---|---|---|---|---|
| Cast Samples | | | | | | | |
| A 2 | 0 | | 0 | | 0 | 4 | 2 |
| C 2 | 5.0-8.5 | | 6 | | 5.1 | 12 | 8 |
| D 2 | 12.5-17.3 | | 16 | | 13.6 | 19 | 13 |
| F 2 | 16.0-21.0 | | 24 | | 30.1 | 30 | 22 |
| K 2 | 6-10 | | 46[f] | | 48.7 | 46[d] | 36 |
| Weld samples[g] | | | | | | | |
| 52 D | | 9.0 | | 9.6 | 8.9 | 13 | 9 |
| 6 B | | 8.5 | | 10.1 | 12.5 | 14 | 10 |
| 8 B | | 13.0 | | 16.3 | 18.7 | 20 | 14 |
| 12 H | | 26.5 | | ≈30 | 26.8 | 23 | 16 |

(a) January, 1973 revision.
(b) Determined at Ohio State University
(c) Duplicate sets of readings were taken on two Magne-Gages, both calibrated using the WRC procedure, and averaged to give the ferrite number. On the cast samples eight readings were taken on each specimen, and on the weld samples four readings down the centerline. The scale for cast metal is different and gives higher values than the scale for weld metal.
(d) Average of two determinations which yielded 44 and 47.
(e) Corrected using the curve of Fig. 6.
(f) The large deviation between the measured ferrite content and that predicted from the diagram is probably related to the relatively high carbon content of this alloy, as explained in the appendix of this article.
(g) Values based on estimated chemistry, not actuals.

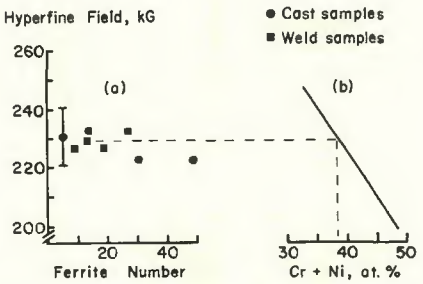


*Fig. 10 — (a) The average magnetic hyperfine field of the ferrite phase, as measured by the Mössbauer effect, plotted as a function of ferrite number.*

*(b) Assumed hyperfine field versus chromium plus nickel content in ternary Fe-Cr-Ni alloys. The dotted line indicates that, based on the assumptions stated in the text, the ferrite phase contains, on the average, about 38 at. % Cr + Ni*

tional corrections for ferrite composition and atomic density give the point at the top of the arrow for the cast sample with the highest ferrite content. Similar corrections would be proportionally smaller for the lower ferrite number samples.

## Comparison With Other Techniques

Gunia and Ratz (Refs. 6,7) have reviewed the methods most commonly used to determine ferrite content in austenitic welds and in cast stainless steels. These methods are divided into three general classes — magnetic, metallographic, and x-ray. They conclude that, for practical purposes, the average ferrite content cannot be determined with a precision greater than about ± 3% ferrite for ferrite levels less than about 10%, and no better than about ± 6% ferrite for ferrite contents from about 10 to 24%. The precision actually obtained will of course depend on many factors, one of the most important of which is instrument calibration. The recently developed ferrite number calibration procedure (Ref. 9) for the Magne-Gage will undoubtedly result in better precision in the use of this instrument for measuring stainless steel welds and castings. However, this procedure does not resolve the potentially important problem of what is the relation of ferrite number to true ferrite content.

Each technique for ferrite determination has its own set of limitations. Among the various techniques, quantitative optical metallography is generally regarded as having the greatest inherent accuracy for sufficiently large and well defined second phases. However, this technique is limited (Ref. 39) by statistical sampling errors, particle edge effects, resolution, and proper phase identification. Note that these problems are particularly important in welds due to the fine distribution of ferrite. For cast materials, the ferrite particles are larger and better defined, resulting in more dependable values from optical metallography. Some of the problems in the use of quantitative metallography specifically for ferrite determination in austenitic stainless steel welds have recently been emphasized by Goodwin et al (Ref. 40).

X-ray diffraction is a technique found to be capable of good accuracy for ferrite determination in wrought stainless steels (Refs. 6,7) with ferrite levels in excess of 3%. The factors involved in an x-ray determination have been summarized by Bechtoldt (Ref. 41). Quantitative results on an absolute basis require corrections for absorption, inhomogenity, particle size, density, and orientation effects. Preferred orientation and coring pose particularly serious impediments for ferrite determinations in stainless steel welds and castings.

The precision of all the conventional magnetic methods with the exception of magnetic saturation depends upon the surface condition of the specimen, the possibility of an air gap between the specimen and the measuring probe, and possible influences of ferrite particle shape and orientation. Since the ferrite content of a weld or cast specimen can vary by an appreciable amount, an average ferrite content is obtained by taking several measurements at different points. The magnetic saturation method does permit, in principle, an absolute determination of ferrite content, provided the saturation magnetization of the ferrite is known. This method is relatively insensitive to the shape, size and orientation of the ferrite particles, although the field required to reach saturation does depend on these factors. As discussed by Bungart et al (Ref. 8) it is necessary to know the relationship between the saturation magnetization and the chemical constitution of the ferrite. It is claimed (Ref. 8) that the relationship has been established for ternary Fe-Ni-Cr, but this should be confirmed by independent measure-

ments. Further, the effects of other alloying elements, even in trace amounts, may limit the precision.

The Mössbauer effect, x-ray and quantitative optical metallography are all basically surface techniques, with the x-ray and Mössbauer probing the sample up to a few mils (1 mil $\approx 25\,\mu$m) below the surface. X-rays and Mössbauer both give an average result for the irradiated sample area, whereas optical metallography requires statistical sampling. The Magne-Gage, another magnetic method, gives an average over a localized region in the vicinity of the tip of a small magnet, but is essentially a low-field method and is sensitive to preferred orientation, ferrite composition and differences in initial permeability of the ferrite particles.

Both the Mössbauer and magnetic saturation methods have the advantage that they make a clear distinction between the magnetic and nonmagnetic phases of the sample being measured. The Mössbauer method has the advantage of being less sensitive to corrections arising from the ferrite composition. However, although it can undoubtedly be improved, the precision of the Mössbauer method is less than that of the magnetic saturation method.

Referring to Fig. 11, the Mössbauer measurements presented here appear to be in essential agreement with the ferrite number for samples containing below about 20% ferrite. Above about 20% ferrite, the ferrite numbers appear to be systematically greater than that indicated by the Mössbauer measurements. The same general trend also appears for the magnetic saturation determinations of Bungart et al (Ref. 8). The data are presently too scanty to draw definite conclusions. It is interesting to note, however, that considerably poorer agreement between percent ferrite and ferrite number would have been obtained here had not the difference in magnetic response for weld and cast materials been taken into account in the WRC procedure (Ref. 9). This difference in response is compensated for by assigning the same ferrite number to the various NBS thickness standards but using different magnets for weld and cast materials. If the weld metals had been rated with the same magnet used for the cast metals, the weld metal ferrite numbers would have been increased by about 22%. This would have, for all the data on weld metals obtained here (see Fig. 11), given considerably poorer agreement between the Mössbauer effect results and the ferrite numbers. Thus the Mössbauer results give additional confirmation that a given amount of ferrite in weld metal is more strongly attracted to a given Magne-Gage magnet than is the same amount of ferrite in cast stainless steel, due presumably to the differences in size, shape, and orientation of the ferrite.

Additional comments about cast stainless steel appear in the Appendix, in connection with the Schoefer diagram for estimating the ferrite content of cast austenitic alloys.

## Conclusions

The present investigation has shown that it is feasible to use Mössbauer-effect scattering methods to obtain baseline information for ferrite content in stainless steel welds and castings. Factors needed to relate the Mössbauer spectral area ratios to the percent ferrite have been developed. The percentage of iron in the ferrite phase can be estimated from the Mossbauer spectrum but more information on the hyperfine fields in ternary and higher alloys is required to improve the reliability of the results. Methods for further development of Mössbauer scattering as a technique for the calibration of other measuring instruments via standard reference materials have been indicated. The preliminary results presented in this paper do not provide a sufficient basis for changes in the presently accepted assignment of ferrite numbers. Intercomparison of the various methods on specially fabricated materials with good homogeneity appears essential.

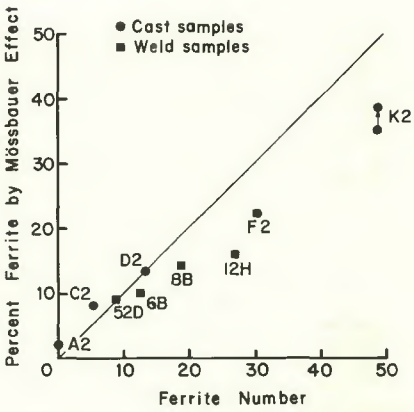


*Fig. 11 — Comparison of ferrite content as measured by the Mössbauer experiments described in this paper, with ferrite number as measured by the Welding Research Council procedure (Ref. 9). Ferrite number has been fixed by WRC (Ref. 9) to correspond with the average commercial practice in 1971-1972. The upper point for the sample with highest ferrite number includes corrections for ferrite composition and atomic density. All other points have been corrected for finite thickness effects only*

*References*


1. Thomas, R. D. Jr., "Crack Sensitivity of Chromium-Nickel Stainless Weld Metal", *Metal Progress* 50, p. 474, 1946.

2. Poole, L. K., "Sigma — An Unwanted Constituent in Stainless Weld Metal", *Metal Progress* 65, p. 108, 1954.

3. Espy, R. H., "What Weld Metal for Type 316L Stainless Steel", *ibid* 86, p. 109, 1964.

4. Flowers, J. W., Beck, F. H., and Fontana, M. G., "Corrosion and Age Hardening Studies of Some Cast Stainless Alloys Containing Ferrite", *Corrosion* 19 (5), pp. 186t-198t, May 1963. Beck, F. H., Schoefer, E. A., Flowers, J. W., and Fontana, M. G., "New Cast High-Strength Alloy Grades by Structure Control", *ASTM STP* 369, Philadelphia, Pa. 1965.

5. Polgary, S., "Resistance to Intercrystalline Corrosion in Stainless Steel Weld Metal", *Svetsaren English Edition* 1-2, p. 2, 1972.

6. Gunia, R. B., and Ratz, G. A., "The Measurement of Delta Ferrite in Austenitic Stainless Steel", *Welding Research Council Bulletin* 132, 1968.

7. Ratz, G. A., and Gunia, R. B., "How Accurate are Methods for Measuring Ferrite?", *Metals Progress*, p. 76, Jan. 1969.

8. Bungart, K., Dietrich, H., and Arntz, H., "The Magnetic Determination of Ferrite in Austenitic Materials, and Especially in Austenitic Welded Material", *DEW-Techn. Ber.* 10, p. 298, 1970.

9. DeLong, W. T., "Calibration Procedure for Instruments to Measure the Delta Ferrite Content of Austenitic Stainless Steel Weld Metal", *Welding Journal* 52 (2), Research Suppl. p. 69s, 1973.

10. Contribution from the French Delegation of the International Institute of Welding, April 21, 1971.

11. Unpublished work done by the Advisory Subcommittee of the High Alloys Committee of the Welding Research Council, 345 East 47th Street, New York, N.Y. 10017, and studies and reports of Subcommission II-C of the International Institute of Welding on Ferrite Measurement.

12. Schwartz, L. H., "Quantitative Analysis Using Mössbauer Effect Spectroscopy", *Int. J. Non-destructive Testing* 1, p. 353, 1970.

13. Weisman, I. D., Swartzendruber, L. J., and Bennett, L. H., "Nuclear Resonances in Metals: Nuclear Magnetic Resonance and Mössbauer Effect", in *Techniques of Metals Research Vol.* 6, E. Passaglia and R. F. Bunshah editors. (Interscience, New York, 1972).

14. Wertheim, G. K., *Mössbauer Effect: Principles and Applications,* (Academic Press, New York, 1964).

15. Albritton, O. W., and Lewis, J. M., "Computer Differentiation of Mössbauer Spectra", *Welding Journal* 50 (7), Research Suppl., p. 327s, July 1971.

16. Chandra, D., and Schwartz, L. H., "Mössbauer Effect Study of the 475 C Decomposition of Fe-Cr", *Met. Trans.* 2, p. 511, 1971.

17. De Nys, T., and Gielen, P. M., "Spinodal Decomposition in the Fe-Cr System", *Met. Trans.* 2, p. 1423, 1971.

18. Yamamoto, H., "A Study of the Nature of Aging in Fe-Cr Alloys by Means of the Mössbauer Effect", *Japan J. Appl. Phys.* 3, p. 745, 1964.

19. Kocher, C. W., "The Iron-57 Mössbauer Effect in Some Stainless Steels", *Phys. Letters* 14, p. 287, 1965.

20. Terrell, J. H., "Backscatter Mössbauer Effect Studies on Steel", *Int. J. of Nondestructive Testing* 2, p. 267, 1970.

21. Lagunov, V. A., Polozenko, and Stepanov, V. A., "Effect of Plastic Deformation on the Mössbauer Effect in Stainless Steel", *Sov. Phys.-Solid State* 11, p. 191, 1969.

22. Lewis, S. J., and Flinn, P. A., "Disappearance of Quadrupole Splitting of the Mössbauer Resonance in Iron-Carbon Austenite at Elevated Temperatures", *Phys. Stat. Sol.* 26, p. K51, 1968.

23. Marcus, H., Schwartz, L. H., and Fine, M. E., "A Study of Precipitation in Stainless and Maraging Steels Using the Mössbauer Effect", *Trans. ASM* 59, p. 468, 1966.

24. Christ, B. W., and Giles, D. M., "On the Detection of Retained Austenite in High-Carbon Steels by Fe-57 Mössbauer Spectroscopy", *Trans. AIME* 242, p. 1915, 1968.

25. Chow, H. K., and Bogner, R. L., "The Study of Retained Austenite by Means of Mössbauer Scattering Spectroscopy", in *Developments in Applied Spectroscopy Vol. 8,* E. L. Grave ed. (Plenum Press, New York, 1970).

26. Fenger, J., "Design of a Simple Mössbauer Resonance Counter", *Nuclear Instr. and Methods* 69, p. 268, 1969.

27. Swartzendruber, L. J., and Bennett, L. H., "Retained Austenite Developed During Surface Grinding of a Carbon Steel", *Scripta Met.* 6, p. 737, 1972.

28. Heberle, J., "Linewidth of Mössbauer Absorption", *Nucl. Instr. and Meth.* 58, p. 90, 1968.

29. Lang, G., "Interpretation of Experimental Mössbauer Spectrum Areas", *ibid* 24, p. 425, 1963.

30. Hofemeister, D. W., and Shera, E. B., "Calculation of Mössbauer Absorption Areas for Thick Absorbers", *ibid* 41, p. 133, 1966.

31. O'Conner, D. A., "The Effect of Line Broadening of Mössbauer Resonant Sources and Absorbers on the Resonant Absorption", *ibid* 21, p. 318, 1963.

32. Ruby, S. L., and Hicks, J. M., "Line Shape in Mössbauer Spectroscopy", *Rev. Sci. Instr.* 33, p. 27, 1963.

33. S. M. Qaim, "Recoil-Free Fraction of the 14.4 keV Mössbauer Gamma Line of Fe-57 in Various Host Lattices", *J. Phys.* F 1, p. 320, 1971.

34. The cast samples were provided by Prof. F. H. Beck of Ohio State University. The weld samples were provided by Teledyne McKay.

35. Chrisman, B. L., and Tumolillo, T. A., "Computer Analysis of Mössbauer Spectra", *Computer Phys. Comm.* 2, p. 322, 1971.

36. Yamamoto, H., "A Study on the Nature of Aging of Fe-Cr Alloys by Means of the Mössbauer Effect", *Japan. J. Appl. Phys.* 3, p. 745, 1964.

37. Johnson, C. E., Ridout, M. S., and Cranshaw, T. E., "Hyperfine Fields in Metals and Alloys", *Proc. 2nd Intl. Conf. Mössbauer Effect,* p. 142, 1961.

38. Pearson, W. B., *Handbook of Lattice Spacings and Structures of Metals and Alloys,* Vol. 2, p. 824 (Pergamon Press, New York, 1967).

39. Moore, G. A., "Is Quantitative Metallography Quantitative?", *ASTM STP* 480, p. 3, Philadelphia, Pa., 1970.

40. Goodwin, G. M., Cole, N. C., and Slaughter, G. M., "A Study of Ferrite Morphologhy in Austenitic Stainless Steel Weldments", *Welding J.* 51 (9), Research Suppl., p. 425s, 1972.

41. Bechtoldt, C. J., "An X-ray Diffraction Method for Determining the Amount of Austenite in an Austenite-Ferrite Mixture", *NBS Technical Note* 709, U.S. Govt. Printing Office, Washington, D.C., 1972.

# APPENDIX

## *One of the authors* presents a one-line constitution diagram for cast alloys and discusses the high ferrite readings obtained with the Mössbauer technique*

The Schoefer diagram (Ref. 1) for the estimation of ferrite percentage in cast austenitic alloy was derived from the Schaeffler diagram (Ref. 2) developed for weld metal. In these diagrams all ferrite-promoting elements are converted into "chromium equivalents" and all austenite-promoting elements into "nickel equivalents" through the use of factors representing the ferritizing or austenitizing power of each element. The following factors are used for the Schoefer diagram:

| Ferritizing | |
|---|---|
| Chromium | 1.0 |
| Silicon | 1.5 |
| Molybdenum | 1.0 |
| Columbium | 1.0 |

| Austenitizing | |
|---|---|
| Nickel | 1.0 |
| Manganese | 0.5 |
| Carbon | 30.0 |
| Nitrogen ($N > 0.02$) | 26.0 |

In addition, the chromium equivalent is *reduced* by a constant of 4.99, and the nickel equivalent is *increased* by a constant of 2.77. The effect of these constants is to transform the coordinates of the Schaeffler diagram so that the origin is at the point where the constant-ferrite lines converge. Thus the ratio of the modified chromium equivalent to the modified nickel equivalent is the reciprocal of the slope of the constant-ferrite lines (see Fig. A1). The reciprocal is chosen to make the composition ratio increase directly with increasing ferrite content. The relationship of composition ratio and ferrite percentage, therefore, is expressed on the Schoefer diagram as a single curve. This is convenient both for estimation of ferrite content, if the composition of an alloy is known, or for selecting aim points for individual elements in calculating the charge for an alloy heat to meet a specified ferrite range.

Whereas ferrite content was stated originally on the diagrams as "ferrite percent", the standardized calibration procedure for magnetic measurement of delta ferrite recently adopted by the Welding Research Council (Ref. 3) designates such quantities in "ferrite numbers". Although closely related, there is some difference between former "ferrite percent" and present "ferrite number" values. Accordingly, the up-to-date version of the Schoefer diagram shown in Fig. A2 has been drawn to reflect this difference.

For an existing alloy, the ferrite content can be estimated by calculating the composition ratio from the chemical analysis and entering the diagram horizontally at the proper level

**E. A. SCHOEFER (see title page) submitted this appendix after the original paper had been presented at the 54th AWS Annual Meeting.*

on the ordinate to the point of intersection with the curve. The corresponding probable range of ferrite number is then determined as follows:

1. A vertical line is drawn from this point to the upper and lower bounds of the scatter band;
2. Horizontal lines are then drawn from these intersection points to the curve;
3. From these points on the curve the ferrite number range can be read on the abscissa, as indicated in Fig. A2.

To calculate a charge for an alloy of the CF-8 type to have, for example, a ferrite number in the range of 10 to 20, it is desirable to select aim points for the elements that will achieve a composition ratio of about 1.265 (read from the curve for 18 FN). The aim ratio should be on the high side of the desired ferrite range since it is easier to lower the ratio than to raise it after a preliminary chemical analysis prior to tapping the heat. The final ratio should be between 1.170 and 1.260 (i.e., between indicated 12.5 and 17.5 FN) in order to allow for uncertainties in the chemical analysis. The initial aim points, therefore, might be as follows:

Cr equivalent

| | | |
|---|---|---|
| Cr | 20.00 × 1.0 | = 20.00 |
| Si | 1.00 × 1.5 | = 1.50 |
| k | | = -4.99 |
| | | 16.51 |

Ni equivalent

| | | |
|---|---|---|
| Ni | 7.50 × 1.0 | = 7.50 |
| Mn | 0.80 × 0.5 | = 0.40 |
| C | 0.06 × 30 | = 1.80 |
| N | (0.04-0.02) × 26 | = 0.52 |
| k | | = 2.77 |
| | | 12.99 |

$$\text{Composition ratio} = \frac{16.51}{12.99} = 1.271$$

If the preliminary analysis shows:

| | | |
|---|---|---|
| Cr | 20.50 × 1.0 | = 20.50 |
| Si | 1.20 × 1.5 | = 1.80 |
| K | | = -4.99 |
| | | 17.31 |

| | | |
|---|---|---|
| Ni | 7.35 × 1.0 | = 7.35 |
| Mn | 0.88 × 0.5 | = 0.44 |
| C | 0.04 × 30 | = 1.20 |
| N estimated+ | | = 0.52 |
| k | | = 2.77 |
| | | 12.28 |

$$\text{Composition ratio} = \frac{17.31}{12.28} = 1.410$$

+Nitrogen is seldom available in preliminary analyses, but usually can be estimated satisfactorily from experience with the same alloy type and melting practice.

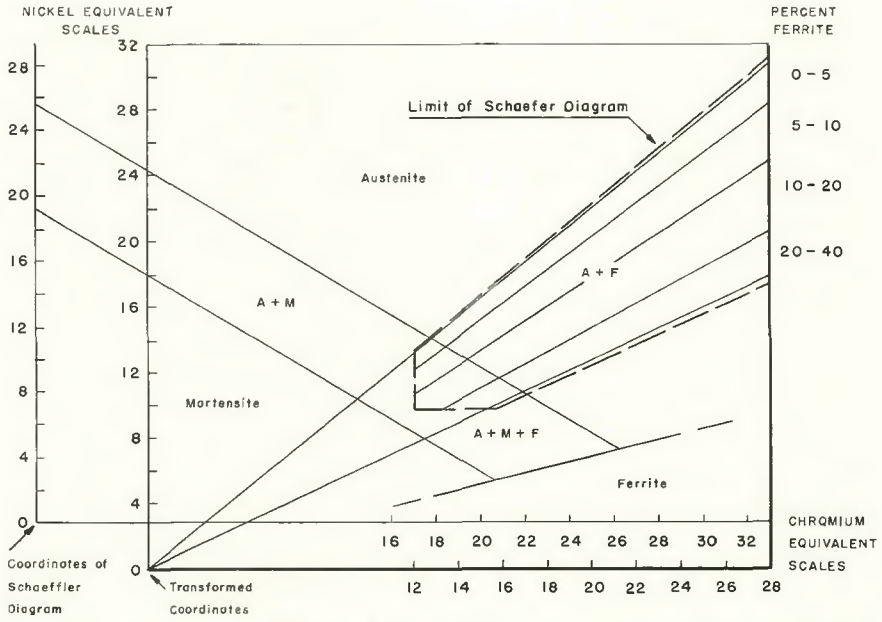


*Fig. A1 — Area of Schaeffler Diagram included in Schoefer Diagram. Transformation of coordinates makes the ratio of chromium equivalent to nickel equivalent to a constant for a given ferrite percentage*

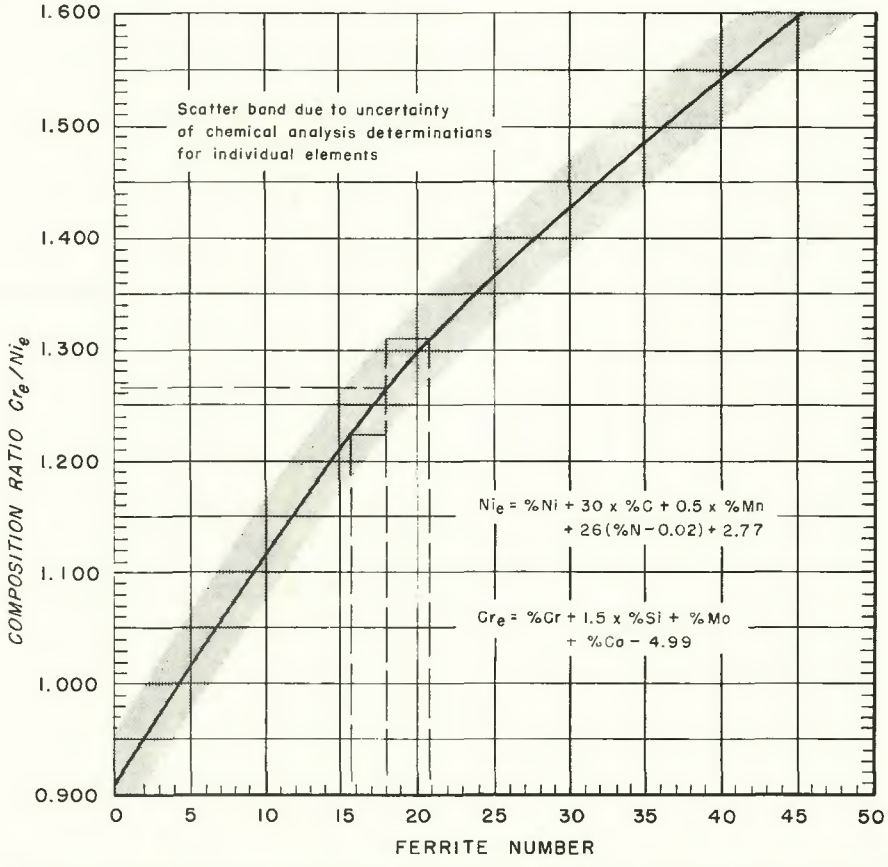


*Fig. A2 — Constitution diagram for estimation of ferrite content in stainless steel castings within the composition range of 16 to 26% chromium, 6 to 14% nickel, 0 to 4% molybdenum, 0 to 1% columbium, up to 0.30% carbon, 0.15% nitrogen, 2.00% manganese, and 2.00% silicon*

The ratio can now be reduced to below 1.260 — the top limit indicated above — by increasing the nickel content. Because nickel recovery is virtually 100%, this is a quick and straightforward calculation. The value of the ratio for 15 FN (the midpoint of the required range) is 1.215, so the nickel equivalent in this case should be:

$$\frac{17.31}{1.215} = 14.25$$

or nickel should be added to increase

the nickel percentage (by 14.25 - 12.28 = 1.97) from 7.35 to 9.32%. This will bring the nickel content within the range (8-11%) specified for the CF-8 alloy type. For a 1,000 lb heat, therefore, the nickel addition is quickly determined to be

$$\frac{19.7}{(1.00 - 0.093)} = 21.7 \text{ lb}$$

For alloys with carbon contents in excess of 0.20%, it is practically impossible to avoid the formation and retention of chromium carbides in castings of normal wall thickness. Even after holding at solution temperatures of 2000-2100 F followed by water quenching, castings of the CE-30 type (26-30Cr, 8-11Ni, 0.30 max C) will have some of the carbon combined with chromium and, as a result, will have a higher ferrite content than would be indicated by consideration of only the amounts of each element in the composition. Although approximately 17 times more weight of chromium than of carbon is tied up in chromium carbide, bound chromium reduces the composition ratio numerator on only a one-to-one basis whereas bound carbon reduces the ratio denominator thirty-to-one. Thus, to the extent that chromium carbides are present, the composition ratio, and hence the ferrite content, is increased.

In as-cast structures, coring occurs and substantial amounts of chromium carbides are formed. Accordingly, wide variations in ferrite content can exist in different areas of as-cast CE-30. This explains the high ferrite of specimen K2 of the Ohio State University series of varied ferrite-content specimens examined by Mössbauer-effect spectroscopy, as shown previously in Table 3. If the composition ratio is computed for the unadjusted chemical analysis of that specimen (Table 1), the chromium equivalent is 25.31, the nickel equivalent is 23.12, and the ratio 1.095, which gives an indicated ferrite content of 6-10% (Table 3), or 7-11 FN. If allowance is made for chromium carbide formation tying up 90% of the available carbon, the Cr and Ni equivalents would be reduced respectively to:

25.31 - 17 × 0.27 =
25.31 - 4.59 = 20.72 and
23.12 - 30 × 0.27 =
23.12 - 8.10 = 15.02

The composition ratio, therefore, would be 20.72/15.02 = 1.379, and the indicated ferrite content 23-29 FN. From Table 3 the average ferrite content of this heat determined metallographically at Ohio State is 46%!

If all the carbon and all but 0.02% of the nitrogen were combined in chromium carbides or carbonitrides, it is readily seen that the Cr and Ni equivalents respectively could be further reduced to:

20.72 - (17 × 0.03 + 8 × 0.10) =
20.72 - 1.31 = 19.41, and
15.02 - (30 × 0.03 + 26 × 0.10) =
15.02 - 3.5 = 11.52

A composition ratio of 1.685 would result which would indicate a ferrite content in excess of 45 FN, so that by segregation during solidification it appears quite possible for ferrite in the quantity observed [48.7 FN] for specimen K2 (Table 3) to occur.

A current research project sponsored by the Alloy Casting Institute Division, Steel Founders' Society of America, at Ohio State University is now being directed toward elucidation of the influence of cooling rates on the occurrence of ferrite in austenitic castings. The effects of subsequent heat treatments on the diffusion of the elements and the solution of minor phases also will be investigated.

*References*


1. Beck, F. H., Schoefer, E. A., Flowers, J. W., and Fontana, M. G., "New Cast High-Strength Alloy Grades by Structure Control", *ASTM Special Technical Publication No. 369,* 1965.

2. Schaeffler, A. L., "Constitution Diagram for Stainless Steel Weld Metal", *Metal Progress,* 680-B, November 1949.

3. DeLong, W. T., "Calibration Procedure for Instruments to Measure the Delta Ferrite Content of Austenitic Stainless Steel Weld Metal", *Welding Journal* 52 (2), Research Suppl. p. 69-s, 1973.